Combustion and Flame 162 (2015) 4514–4522

Contents lists available at ScienceDirect

Combustion and Flame

journal homepage: www.elsevier.com/locate/combustflame

Gibbs function continuation for linearly constrained multiphase equilibria

James B. Scoggins[1,*], Thierry E. Magin[1]

Aeronautics and Aerospace Department, von Karman Institute for Fluid Dynamics, Rhode-Saint-Genese, Belgium

ARTICLE INFO

Article history:
Received 28 April 2015
Revised 29 July 2015
Accepted 31 August 2015
Available online 21 October 2015

Keywords:
Chemical equilibrium
Multiphase equilibria
Gibbs function continuation
Element Potential Equations

ABSTRACT

The stable computation of linearly constrained, multiphase, chemical equilibrium compositions is an important topic for a wide range of industrial and academic applications. Numerous computational methods have been developed to solve such problems which are, in general, susceptible to failure under certain conditions due to numerical stiffness. In this work, we present a Gibbs function continuation method for linearly constrained multiphase equilibrium calculations. The method converts the nonlinear Element Potential Equations - derived from the minimization of the mixture Gibbs free energy using the Lagrange multiplier technique - into an initial value problem which can be stably integrated through the use of a property of linear least squares solutions. The stability and convergence properties of the proposed method are derived and it is shown that the single phase method arises as a special case of the multiphase algorithm when only one phase is considered. Two test cases are presented to clarify and demonstrate the accuracy and robustness of the method.

1. Introduction

The efficient and robust computation of multiphase, constrained equilibrium compositions is an important topic over a wide range of fields including combustion, aerospace and (bio)chemical engineering, metallurgy, paper processes, and the design of thermal protection systems for atmospheric entry vehicles (e.g., [1–6]). For a detailed history and list of applications, the reader is referred to the treatises by van Zeggeren and Storey [7] or Smith and Missen [8].

Prior to the work of White et al. [9], the equilibrium constant formulation was primarily used to compute equilibrium compositions for ideal, gas phase mixtures. The equilibrium constant formulation works by assigning formation reactions to each species based on a set of base or component species which are chosen *a priori* for the given reaction system. Kuo [10] cites several disadvantages that hindered researches using this method including difficulties in extending the method to non ideal equations of state, testing for the presence of condensed species and numerical complications with the use of component species.

In 1958, White et al. [9] introduced the concept of free-energy minimization and proposed a numerical solution technique using the method of steepest decent. White [11] later elaborated on the advantages of free-energy minimization and the use of element potentials in the solution of equilibrium compositions, including the possibility to treat any general chemical system without the necessity of specifying the formation reactions. In addition, the use of element potentials allowed for the solution of linear systems whose size scaled with the number of elements rather than species, present in the mixture. This fact alone offers a significant computational advantage when considering large chemical systems.

Today, both the equilibrium constant formulation and the free-energy minimization methods are widely used. Most commercial and general purpose research codes implement various numerical methods for solving the free-energy minimization problem, however the equilibrium constant formulation is still used in certain applications [4,12]. Perhaps one of the most widely used equilibrium codes today is the Stanford-JANAF (STANJAN) code by Reynolds [13] who popularized the element potential method for constrained Gibbs free-energy minimization by developing a numerical solution procedure to the minimization problem which solves the so-called dual problem. Part of the success of the STANJAN method lies in its powerful initialization and preconditioning procedures which help make STANJAN extremely robust for most problems. The Chemical Equilibrium with Applications (CEA) code developed by Gordon and McBride [14,15] is also used heavily, helped by the success of the detailed thermodynamic database developed at NASA Glenn Research Center [16], which it employs.

In addition to the normal mass balance constraints, so called "generalized constraints" [17] on the equilibrium solution have been used in a wide range of applications [3] and in particular, are an integral component of the Rate-Controlled Constrained Equilibrium (RCCE)

* Corresponding author.
E-mail addresses: scoggins@vki.ac.be (J.B. Scoggins), magin@vki.ac.be (T.E. Magin).
[1] Also at Laboratoire EM2C, Ecole Centrale Paris, France.

http://dx.doi.org/10.1016/j.combustflame.2015.08.027
0010-2180/

[17–31] method. Some important examples of constraints used in the RCCE method include constraints on the total number of moles, the number of free valence electrons, and the number of O-O bonds, among many others [3,30]. Bishnu et al. [32,33] added the ability to include general linear constraints on the equilibrium solutions to both STANJAN and CEA. They found that, under certain conditions, both the constrained versions of STANJAN and CEA failed to converge to a solution. In general, these situations arise when the linear constraints force the equilibrium composition near the boundary of the feasible region imposed by the hyperplane defined by the constraints.

In an effort to provide a provably robust, constrained equilibrium solver, Pope [34,35] developed the Gibbs Function Continuation (GFC) method which solves the Element Potential Equations for an ideal gas mixture under general linear constraints. Since its development, the GFC method has been successfully embedded into a variety of more complex turbulent combustion modeling algorithms, including the eddy dissipation concept (EDC) [36,37], RCCE using a greedy algorithm with local improvement (RCCE-GALI) [29], and the Relaxation–Redistribution method (RRM) [38]. One drawback of the GFC method however, is that it is only capable of computing equilibrium compositions of gas phase mixtures.

The purpose of this paper is to generalize the GFC method to mixtures with multiple ideal phases and to provide a more rigorous mathematical analysis of its robustness and stability. The new method is referred to as the multiphase Gibbs function continuation (MPGFC) method. In Section 2, the necessary equations to describe constrained chemical equilibrium for any number of ideal phases are reviewed. Section 3 develops the mathematical basis of the MPGFC method, followed by a detailed overview of a practical implementation of the algorithm in Section 4. Finally, two numerical test cases will be presented to demonstrate some key features of the algorithm in Section 5 before a few concluding remarks.

2. Constrained chemical equilibrium

2.1. Free energy minimization

Consider a chemical system composed of any number of ideal phases. The set of indices which denote all species in this system is $\mathcal{S} = \{1, \ldots, n^{\mathcal{S}}\} = \cup_{m\in\mathcal{P}}\mathcal{S}_m$ where $n^{\mathcal{S}}$ is the total number of species considered, $\mathcal{P} = \{1, \ldots, n^{\mathcal{P}}\}$ is the set of phase indices with $n^{\mathcal{P}}$ the number of phases, and $\mathcal{S}_m$ denotes the set of species indices belonging to phase m. Note that each species belongs to a single phase. If a particular chemical species occurs in (for example) three phases, then it is treated as three different species. Since all phases are ideal, the normalized Gibbs function for this system is

$$\tilde{G} \equiv \frac{G}{RT} = \sum_{m\in\mathcal{P}}\sum_{j\in\mathcal{S}_m} N_j\left(\tilde{g}_j + \ln N_j - \ln \bar{N}_m\right), \tag{1}$$

where N_j is the number of moles of species j and $\tilde{g}_j(T, p)$ is the non-dimensional Gibbs function of pure species j at the system temperature T and pressure p, R is the molar universal gas constant, and $\bar{N}_m$ is the total moles in phase m, sometimes referred to as the phase moles of phase m.

$$\bar{N}_m = \sum_{j\in\mathcal{S}_m} N_j, \quad \forall\, m \in \mathcal{P}. \tag{2}$$

The vector of $n^{\mathcal{P}}$ phase moles, $\bar{\boldsymbol{N}}$, can thus be expressed as

$$\bar{\boldsymbol{N}} = \mathbf{P}^T\boldsymbol{N}, \tag{3}$$

where $\boldsymbol{N} \in \mathbb{R}^{n^{\mathcal{S}}}$ is the vector of species moles and $\mathbf{P} \in \mathbb{R}^{n^{\mathcal{S}}\times n^{\mathcal{P}}}$ is a "phase summation matrix" whose elements are defined as

$$P_{jm} \equiv \delta_{p_j m}. \tag{4}$$

The symbol $\delta_{p_j m}$ is the familiar Kronecker Delta function and the subscript p_j is used to denote the index of the phase in $\mathcal{P}$ to which the species j belongs. In other words, for all m in $\mathcal{P}$ and all j in $\mathcal{S}_m$, $p_j = m$.

Table 1
Example constraint matrices **B** and **P** for a 5-species CO_2 mixture with constraints placed on the total mixture moles, $\bar{N}_{\text{mix}}$.

	B columns			**P** columns	
Species	C	O	$\bar{N}_{\text{mix}}$	Gas	C(gr)
C	1	0	1	1	0
CO	1	1	1	1	0
CO_2	1	2	1	1	0
O_2	0	2	1	1	0
C(gr)	1	0	1	0	1

The two notations of the phase index are used for convenience, depending on the situation. For instance, Eq. (1) may be equivalently written as

$$\tilde{G} = \sum_{j\in\mathcal{S}} N_j\left(\tilde{g}_j + \ln N_j - \ln \sum_{k\in\mathcal{S}_{p_j}} N_k\right). \tag{5}$$

The non-dimensional Gibbs function for a pure species j is given by

$$\tilde{g}_j(T, p) = \frac{H_j(T)}{RT} - \frac{S_j^\circ(T)}{R} + \begin{cases} \ln\dfrac{p}{p^\circ}, & j \in \text{gas phase} \\ 0, & \text{otherwise} \end{cases}, \tag{6}$$

where H_j is the molar enthalpy of pure species j and S_j°, its molar entropy evaluated at the standard state pressure p°.

If the total moles of each element i in the mixture is denoted by c_i^{e}, then conservation of mass dictates that

$$\sum_{j\in\mathcal{S}} B_{ji}^{\text{e}} N_j = c_i^{\text{e}} \quad \forall\, i \in \mathcal{E}, \tag{7}$$

where B_{ji}^{e} is the stoichiometric coefficient for the ith element in species j. $\mathcal{E} = \{1, \ldots, n^{\mathcal{E}}\}$ denotes the set of element indices for the $n^{\mathcal{E}}$ considered elements in the mixture. Eq. (7) is often referred to as the mass balance relations or constraints. It states that the available atoms in a mixture must be shared amongst each of the species in the mixture (regardless of phase). In addition to these physically imposed constraints, it is often useful to impose other constraints on the system. Therefore, we consider the set of $n^{\mathcal{G}}$ additional linear constraints on the number of moles of each species, $\mathcal{G} = \{1, \ldots, n^{\mathcal{G}}\}$, such that

$$\sum_{j\in\mathcal{S}} B_{ji}^{\text{g}} N_j = c_i^{\text{g}} \quad \forall\, i \in \mathcal{G}. \tag{8}$$

Using matrix notation, the total constraints imposed on the composition are thus given by

$$\mathbf{B}^T\boldsymbol{N} = \boldsymbol{c}, \tag{9}$$

where

$$\mathbf{B} = \begin{bmatrix}\mathbf{B}^{\text{e}} & \mathbf{B}^{\text{g}}\end{bmatrix} \in \mathbb{R}^{n^{\mathcal{S}}\times n^{\mathcal{C}}}, \quad \boldsymbol{c} = \begin{bmatrix}\boldsymbol{c}^{\text{e}} \\ \boldsymbol{c}^{\text{g}}\end{bmatrix} \in \mathbb{R}^{n^{\mathcal{C}}}, \tag{10}$$

and $n^{\mathcal{C}} = n^{\mathcal{E}} + n^{\mathcal{G}}$ are the total number of linear constraints whose indices compose the set $\mathcal{C} = \{1, \ldots, n^{\mathcal{C}}\}$. As a clarifying example, consider a 5-species mixture composed of four gaseous species, C, CO, CO_2, and O_2, and solid graphite, C(gr), with an imposed constraint on the total mixture moles, $\bar{N}_{\text{mix}}$. Table 1 shows the corresponding **B** and **P** matrices associated with this system. Note that the first two columns of **B** correspond to the mass balance constraints in Eq. (7) while the last column corresponds to the constraint on the total mixture moles.

For a given **B**, $\boldsymbol{c}$, and a fixed temperature and pressure, the local thermodynamic equilibrium (LTE) composition for a chemical system is the one which minimizes $\tilde{G}$, Eq. (1), while satisfying the linear constraints in Eq. (9).

2.2. Constraint potentials

The Lagrange multiplier method is a well known technique for solving constrained minimization problems and will be used here. To

begin, the Gibbs function and mass balance constraints are combined to form the Lagrangian, L,

$$L = \tilde{G} - \sum_{i\in\mathcal{C}} \lambda_i \left(\sum_{j\in\mathcal{S}} B_{ji} N_j - c_i \right)$$
$$= \sum_{j\in\mathcal{S}} N_j \left(\tilde{g}_j + \ln N_j - \ln \sum_{k\in\mathcal{S}_{p_j}} N_k \right) - \sum_{i\in\mathcal{C}} \lambda_i \left(\sum_{j\in\mathcal{S}} B_{ji} N_j - c_i \right) \quad (11)$$

through the use of Lagrange multipliers, λ_i. Setting the derivative of the Lagrangian with respect to the species moles to zero provides the necessary conditions for the solution of the minimization problem. Namely,

$$\frac{\partial L}{\partial N_j} = \frac{\partial \tilde{G}}{\partial N_j} - \sum_{i\in\mathcal{C}} \lambda_i B_{ji}$$
$$= \tilde{g}_j + \ln N_j - \ln \sum_{k\in\mathcal{S}_{p_j}} N_k - \sum_{i\in\mathcal{C}} \lambda_i B_{ji}$$
$$= 0, \quad \forall\, j \in \mathcal{S}. \quad (12)$$

The physical meaning of the Lagrange multipliers is evident when Eq. (11) is differentiated with respect to the constraint constants, c_i, yielding

$$\frac{\partial L}{\partial c_i} = \frac{\partial \tilde{G}}{\partial c_i} + \lambda_i = 0 \Rightarrow \lambda_i = -\frac{\partial \tilde{G}}{\partial c_i}. \quad (13)$$

Therefore, λ_i is a dimensionless number which represents the negative rate of change in the normalized Gibbs energy of the equilibrium system with respect to a change in the constraint constant, c_i. In addition, Eq. (12) may be rewritten such that

$$\sum_{i\in\mathcal{C}} \lambda_i B_{ji} = \frac{\partial \tilde{G}}{\partial N_j} \equiv \frac{\mu_j}{RT}, \quad \forall\, j \in \mathcal{S}, \quad (14)$$

where μ_j is called the chemical potential of species j for the given chemical system. Because of this relationship, the Lagrange multipliers are often referred to as element potentials when they are associated with elemental mass balance constraints, or simply constraint potentials for a general constraint.

Finally, Eq. (12) may also be rewritten to yield the Element Potential Equations (EPE's) [13],

$$N_j = \bar{N}_{p_j} \exp\left(-\tilde{g}_j + \sum_{i\in\mathcal{C}} \lambda_i B_{ji} \right), \quad \forall j \in \mathcal{S}, \quad (15)$$

which show that the number of moles of each species, N_j, in a mixture at equilibrium are functions of only their phase moles, $\bar{N}_{p_j}$, and the $n^{\mathcal{C}}$ constraint potentials, λ_i, corresponding to each constraint i. Note that when written in terms of species mole fractions, $x_j = N_j/\bar{N}_{p_j}$, the constraint potentials λ_i completely define the equilibrium composition of each phase for a fixed temperature and pressure (but not the amount of each phase present in the mixture). Substitution of Eq. (15) into Eqs. (3) and (9) leads to a nonlinear system of $n^{\mathcal{P}} + n^{\mathcal{C}}$ equations and as many unknowns: $\bar{N}_m$, $\forall\, m \in \mathcal{P}$, and λ_i, $\forall\, i \in \mathcal{C}$. The robust solution of this nonlinear system is the focus of the following sections.

2.3. Coordinate transformation and matrix-vector representation

The following sections make use of a coordinate transformation which simplifies the development of the multiphase Gibbs function continuation method. This transformation is similar to the one made by Pope in the original development of the single-phase method. Instead of dealing directly with species moles, it is convenient to use their square-root,

$$y_i \equiv \sqrt{N_i}. \quad (16)$$

The purpose of this change of variables will become evident later. Using Eq. (15), the vector $\boldsymbol{y} \in \mathbb{R}^{n^{\mathcal{S}}}$ may be expressed in matrix-vector notation as a function of the element potential vector, $\boldsymbol{\lambda} \in \mathbb{R}^{n^{\mathcal{C}}}$, and phase mole vector $\bar{\boldsymbol{N}} \in \mathbb{R}^{n^{\mathcal{P}}}$ by

$$\boldsymbol{y} = \exp\left(-\tilde{\boldsymbol{g}} + \mathbf{B}\boldsymbol{\lambda} + \mathbf{P} \ln \bar{\boldsymbol{N}} \right)^{\frac{1}{2}}. \quad (17)$$

Here, the exponential, logarithm, and square-root operators act element-wise on their vector argument. Note also that $\mathbf{P}$ in Eq. (17) is used to transform the $n^{\mathcal{P}}$-sized vector $\ln \bar{\boldsymbol{N}}$ into a $n^{\mathcal{S}}$-sized vector with repeated values depending on the phase of each species. This construction will be used throughout the paper. Finally, the matrices $\mathbf{Y} \in \mathbb{R}^{n^{\mathcal{S}} \times n^{\mathcal{S}}}$, $\tilde{\mathbf{B}} \in \mathbb{R}^{n^{\mathcal{S}} \times n^{\mathcal{C}}}$, and $\tilde{\mathbf{P}} \in \mathbb{R}^{n^{\mathcal{S}} \times n^{\mathcal{P}}}$ are defined as

$$\mathbf{Y} \equiv \operatorname{diag}(\boldsymbol{y}), \quad \tilde{\mathbf{B}} \equiv \mathbf{Y}\mathbf{B}, \quad \tilde{\mathbf{P}} \equiv \mathbf{Y}\mathbf{P}. \quad (18)$$

Using the above notation, the constrained chemical equilibrium problem defined in Eqs. (3) and (9) may be written as

$$\tilde{\mathbf{P}}^T \boldsymbol{y} = \bar{\boldsymbol{N}} \quad (19)$$

$$\tilde{\mathbf{B}}^T \boldsymbol{y} = \boldsymbol{c} \quad (20)$$

3. Multiphase Gibbs function continuation

Newton's method, or a variant thereof, is the most common method for solving nonlinear equations such as Eqs. (19) and (20). In general, the convergence of Newton's method for a Lipschitz continuous, nonlinear system, $\boldsymbol{F}(\boldsymbol{x}) = 0$, is q-quadratic when the initial iterate, $\boldsymbol{x}^0$, is close enough to a root of $\boldsymbol{F}$, $\boldsymbol{x}^*$, and the system Jacobian within the region around the root is nonsingular [39]. In fact, quadratic convergence is only guaranteed when the initial guess, $\boldsymbol{x}^0$, is close enough to the real solution, $\boldsymbol{x}^*$, to satisfy the condition

$$\|\boldsymbol{x}^0 - \boldsymbol{x}^*\|_2 < \frac{\|\mathbf{F}'(\boldsymbol{x}^*)\|_2}{\gamma\, \kappa(\mathbf{F}'(\boldsymbol{x}^0))}, \quad (21)$$

where $\mathbf{F}'(\boldsymbol{x})$ is the system Jacobian evaluated at $\boldsymbol{x}$, γ is the Lipschitz constant for $\mathbf{F}'$, and $\kappa(\mathbf{F}'(\boldsymbol{x}))$ is the condition number of $\mathbf{F}'(\boldsymbol{x})$. The condition number is a measure of how close a matrix is to being singular, increasing to infinity when the matrix is singular. Thus, as the Jacobian of the system approaches a singular matrix, the corresponding bound on the initial guess's proximity to the actual solution becomes nearly zero. For the equilibrium problem of Eqs. (19) and (20), situations often arise in which the system Jacobian approaches a singular matrix causing the Newton convergence to stagnate.

The multiphase Gibbs function continuation method avoids the above difficulties by converting Eqs. (19) and (20) into an initial value problem which may be integrated robustly through the use of a continuation parameter. To begin, the multiphase residual vector, $\boldsymbol{R} \in \mathbb{R}^{n^{\mathcal{C}}+n^{\mathcal{P}}}$, is formally expressed as a function of the solution vector, $\tilde{\boldsymbol{x}}$, and the Gibbs vector, $\tilde{\boldsymbol{g}}(T, p)$, such that

$$\boldsymbol{R}(\tilde{\boldsymbol{x}}, \tilde{\boldsymbol{g}}) = \begin{bmatrix} \tilde{\mathbf{B}}^T \\ \tilde{\mathbf{P}}^T \end{bmatrix} \boldsymbol{y} - \begin{bmatrix} \boldsymbol{c} \\ \bar{\boldsymbol{N}} \end{bmatrix}, \quad \text{and} \quad \tilde{\boldsymbol{x}} \equiv \begin{bmatrix} \boldsymbol{\lambda} \\ \ln \bar{\boldsymbol{N}} \end{bmatrix}, \quad (22)$$

where $\tilde{\mathbf{B}}$, $\tilde{\mathbf{P}}$, and $\boldsymbol{y}$ are implicit functions of $\tilde{\boldsymbol{x}}$ as shown in Eqs. (17) and (18). Eqs. (19) and (20) may now be written in terms of the residual vector as $\boldsymbol{R}(\tilde{\boldsymbol{x}}^*, \tilde{\boldsymbol{g}}) = 0$, which implicitly defines the equilibrium point $\tilde{\boldsymbol{x}}^*$ for a fixed T and p. The solution of this nonlinear system via Newton's method is not guaranteed to succeed, based on the arguments made above. Instead, we define a new Gibbs energy vector $\hat{\boldsymbol{g}}$, linearly parameterized by a continuation parameter s, such that

$$\hat{\boldsymbol{g}}(s) = \hat{\boldsymbol{g}}(0) + s\left[\tilde{\boldsymbol{g}} - \hat{\boldsymbol{g}}(0) \right], \quad (23)$$

where $\hat{\boldsymbol{g}}(0)$ denotes $\hat{\boldsymbol{g}}$ at $s = 0$. Replacing $\tilde{\boldsymbol{g}}$ with $\hat{\boldsymbol{g}}$, the equation $\boldsymbol{R}(\hat{\boldsymbol{x}}, \hat{\boldsymbol{g}}(s)) = 0$ now implicitly defines a path of pseudo-equilibrium points $\hat{\boldsymbol{x}}(s)$, parameterized by s, where $\hat{\boldsymbol{x}}(1) = \tilde{\boldsymbol{x}}^*$. As $\hat{\boldsymbol{g}}(0)$ is arbitrary, there are an infinite number of such paths, however, given a set of initial values of $\hat{\boldsymbol{g}}(0)$ and $\hat{\boldsymbol{x}}(0)$ which satisfy $\boldsymbol{R}(\hat{\boldsymbol{x}}(0), \hat{\boldsymbol{g}}(0)) = \mathbf{0}$, the equilibrium point can be determined by tracing the path of pseudo-equilibrium points from $s = 0$ to $s = 1$, via

$$\tilde{\boldsymbol{x}}^* = \hat{\boldsymbol{x}}(1) = \int_0^1 \frac{d\hat{\boldsymbol{x}}}{ds} ds + \hat{\boldsymbol{x}}(0), \quad (24)$$

where the tangent vector, $d\hat{\boldsymbol{x}}/ds = [d\boldsymbol{\lambda}/ds, d\ln\tilde{\boldsymbol{N}}/ds]^T$, can be derived from the implicit relation $d\boldsymbol{R}(\hat{\boldsymbol{x}}, \hat{\boldsymbol{g}}(s))/ds = 0$. Note that the 'hat' symbol is left off of λ and $\tilde{\boldsymbol{N}}$ for convenience but their dependence on s will be clear based on the context. Given a $\hat{\boldsymbol{g}}(0)$, the path $\hat{\boldsymbol{x}}(s)$ is smooth and unique because $\hat{\boldsymbol{g}}(s)$ is linear from Eq. (23) and the existence and uniqueness of the equilibrium problem is well known (see for example [40]).

In its most basic form, the MPGFC method solves for the equilibrium point $\tilde{\boldsymbol{x}}^*$ by numerically integrating the initial value problem of Eq. (24) using a simple Euler scheme. The derivatives, $d\boldsymbol{\lambda}/ds$ and $d\ln\tilde{\boldsymbol{N}}/ds$, can be computed robustly by exploiting a feature of least-squares solutions. In addition, special care must be taken to ensure that the correct condensed phases are included in the equilibrium solution. Further improvements to the efficiency and global accuracy of the method are obtained by using an adaptive step-size, Δs, as well as Newton's method (when possible) to reduce errors in the numerical integration. The mathematical basis for each of these issues are presented in the following subsections while Section 4 will detail the exact MPGFC solution algorithm.

3.1. Initial conditions

The initial conditions, $\hat{\boldsymbol{g}}(0)$, $\boldsymbol{\lambda}(0)$, and $\ln\tilde{\boldsymbol{N}}(0)$, must satisfy the constraint $\boldsymbol{R}(\hat{\boldsymbol{x}}(0), \hat{\boldsymbol{g}}(0)) = \boldsymbol{0}$. Therefore, the initial species moles vector, $\boldsymbol{N}(0)$, must satisfy Eqs. (19) and (20). There are an infinite number of species mole vectors which can satisfy the underdetermined constraint system in Eq. (20). The vector space of all such vectors will be denoted by

$$\mathcal{B} = \left\{\boldsymbol{N} \in \mathbb{R}^{n^S} \;:\; \mathbf{B}^T\boldsymbol{N} = \boldsymbol{c},\; N_j \geq 0\right\}. \tag{25}$$

We now define two species compositions contained in this vector space. The Min-G composition,

$$\boldsymbol{N}_{\text{min-g}} = \arg\min_{\boldsymbol{N}\in\mathcal{B}} \boldsymbol{N}^T\tilde{\boldsymbol{g}}, \tag{26}$$

minimizes the sum of species Gibbs energies while satisfying the constraints in Eq. (20), approximating the minimization of Eq. (1) without regard to the energy of mixing. The Max–Min composition,

$$\boldsymbol{N}_{\text{max-min}} = \arg\max_{\boldsymbol{N}\in\mathcal{B}} \left(\min_{j\in\mathcal{S}} N_j\right), \tag{27}$$

is the composition which maximizes the smallest single species moles and still satisfies Eq. (20). Both compositions can be formulated as the solution to a linear programming problem which can be easily solved via the Simplex algorithm [41]. The Min-G composition is useful because it estimates the equilibrium moles of the major species. However, at most n^C species in $\boldsymbol{N}_{\text{min-g}}$ will be non-zero, while the rest are exactly zero. The Max–Min composition is strictly positive but far from the equilibrium composition as it does nothing to minimize $\tilde{G}$. Therefore, Pope [34] has suggested that a linear combination of the Min-G and Max–Min compositions,

$$\boldsymbol{N}(0) = \boldsymbol{N}_{\text{min-g}}(1-\alpha) + \boldsymbol{N}_{\text{max-min}}\alpha, \tag{28}$$

provides a good approximation of the major equilibrium species while ensuring that all species moles are strictly positive and that Eq. (20) is satisfied. The value of α is typically taken to be 0.01 such that the Min-G composition dominates, and the major species moles are still well approximated by the initial solution.

The Gibbs phase rule [42] says that, for a fixed temperature and pressure, the maximum number of phases allowed in an equilibrium solution are the total number of constraints imposed on it, n^C. In order to ensure that the initial conditions satisfy the phase rule, only the phases which have non-zero moles in the Min-G solution are kept for the Max–Min solution. As the maximum number of non zero species in the Min-G solution is equal to the number of constraints, this is sufficient to ensure the phase rule is satisfied.

Eq. (19) is then directly satisfied by taking

$$\ln\tilde{\boldsymbol{N}}(0) = \ln\left(\mathbf{P}^T\boldsymbol{N}(0)\right). \tag{29}$$

Note the necessity of having a strictly positive $\boldsymbol{N}(0)$ in order for the logarithm above to be well defined.

Eqs. (28) and (29) ensure that $\boldsymbol{R} = 0$ (recall that $\boldsymbol{y} = \sqrt{\boldsymbol{N}}$ from Eq. (16)). All that remains is to determine $\hat{\boldsymbol{g}}(0)$ and $\boldsymbol{\lambda}(0)$ which are consistent with $\boldsymbol{N}(0)$ through the EPE, Eq. (17). First, $\boldsymbol{\lambda}(0)$ is computed as the least-squares solution of the EPE using the Gibbs energy vector, $\tilde{\boldsymbol{g}}$.

$$\boldsymbol{\lambda}(0) = \arg\min_{\boldsymbol{\lambda}} \left\|\mathbf{B}\boldsymbol{\lambda} - \ln\boldsymbol{N}(0) + \mathbf{P}\ln\tilde{\boldsymbol{N}}(0) - \tilde{\boldsymbol{g}}\right\|_2 \tag{30}$$

Finally, $\hat{\boldsymbol{g}}(0)$ is chosen such that Eq. (17) is exactly satisfied.

$$\hat{\boldsymbol{g}}(0) = \mathbf{B}\boldsymbol{\lambda}(0) - \ln\boldsymbol{N}(0) + \mathbf{P}\ln\tilde{\boldsymbol{N}}(0) \tag{31}$$

3.2. Computing $\mathrm{d}\boldsymbol{\lambda}/\mathrm{d}s$ and $d\ln\tilde{\boldsymbol{N}}/ds$

The derivatives, $d\boldsymbol{\lambda}/ds$ and $d\ln\tilde{\boldsymbol{N}}/ds$, at constant $\boldsymbol{R}$, are obtained from the implicit relations found when the residual is differentiated with respect to s and set equal to zero, such that

$$\frac{d\boldsymbol{R}}{ds} = \frac{d}{ds}\begin{bmatrix}\tilde{\mathbf{B}}^T\boldsymbol{y} \\ \tilde{\mathbf{P}}^T\boldsymbol{y} - \tilde{\boldsymbol{N}}\end{bmatrix} = \boldsymbol{0}. \tag{32}$$

From Eq. (17), the following relationship can be easily determined.

$$\begin{aligned}\frac{d}{ds}(\mathbf{Y}\boldsymbol{y}) &= \mathbf{Y}^2\left[\mathbf{B}\frac{d\boldsymbol{\lambda}}{ds} - \frac{d\hat{\boldsymbol{g}}}{ds} + \mathbf{P}\frac{d}{ds}(\ln\tilde{\boldsymbol{N}})\right] \\ &= \mathbf{Y}\left[\tilde{\mathbf{B}}\frac{d\boldsymbol{\lambda}}{ds} - \mathbf{Y}\frac{d\hat{\boldsymbol{g}}}{ds} + \tilde{\mathbf{P}}\frac{d}{ds}(\ln\tilde{\boldsymbol{N}})\right]\end{aligned} \tag{33}$$

Note that $d\hat{\boldsymbol{g}}/ds$ is a known function from Eq. (23), namely $d\hat{\boldsymbol{g}}/ds = \tilde{\boldsymbol{g}} - \hat{\boldsymbol{g}}(0)$. Using Eq. (33), the first term in Eq. (32) can be written as

$$\frac{d}{ds}(\tilde{\mathbf{B}}^T\boldsymbol{y}) = \tilde{\mathbf{B}}^T\left[\tilde{\mathbf{B}}\frac{d\boldsymbol{\lambda}}{ds} - \mathbf{Y}\frac{d\hat{\boldsymbol{g}}}{ds} + \tilde{\mathbf{P}}\frac{d}{ds}(\ln\tilde{\boldsymbol{N}})\right]. \tag{34}$$

We now seek a $d\boldsymbol{\lambda}/ds$ such that $d(\tilde{\mathbf{B}}^T\boldsymbol{y})/ds = \boldsymbol{0}$ is satisfied regardless of the value of $d\ln\tilde{\boldsymbol{N}}/ds$. To begin, $d\boldsymbol{\lambda}/ds$, is decomposed into two components,

$$\frac{d\boldsymbol{\lambda}}{ds} = \dot{\boldsymbol{\lambda}}^g - \dot{\boldsymbol{\Lambda}}^{\boldsymbol{y}}\frac{d}{ds}(\ln\tilde{\boldsymbol{N}}), \tag{35}$$

where $\dot{\boldsymbol{\lambda}}^{\boldsymbol{g}} \in \mathbb{R}^{n^C}$ and $\dot{\boldsymbol{\Lambda}}^{\boldsymbol{y}} \in \mathbb{R}^{n^C\times n^P}$ are obtained via the minimum-norm solutions to the following least-squares problems

$$\dot{\boldsymbol{\lambda}}^g = \arg\min_{\dot{\boldsymbol{\lambda}}} \left\|\tilde{\mathbf{B}}\dot{\boldsymbol{\lambda}} - \mathbf{Y}\frac{d\hat{\boldsymbol{g}}}{ds}\right\|_2, \tag{36}$$

$$\dot{\boldsymbol{\Lambda}}^{\boldsymbol{y}} = \arg\min_{\dot{\boldsymbol{\Lambda}}} \left\|\tilde{\mathbf{B}}\dot{\boldsymbol{\Lambda}} - \tilde{\mathbf{P}}\right\|_2. \tag{37}$$

The solutions of Eqs. (36) and (37) may be stably computed using the singular value decomposition of $\tilde{\mathbf{B}}$, regardless of its rank. In addition, their residuals reside in the null space of $\tilde{\mathbf{B}}^T$, based on a general property of least squares solutions. Thus,

$$\tilde{\mathbf{B}}^T\left(\tilde{\mathbf{B}}\dot{\boldsymbol{\lambda}}^g - \mathbf{Y}\frac{d\hat{\boldsymbol{g}}}{ds}\right) = \boldsymbol{0}, \tag{38}$$

$$\tilde{\mathbf{B}}^T(\tilde{\mathbf{B}}\dot{\boldsymbol{\Lambda}}^{\boldsymbol{y}} - \tilde{\mathbf{P}}) = \boldsymbol{0}. \tag{39}$$

Using this fact and substituting Eq. (35) into Eq. (34) and rearranging, we then have

$$\tilde{\mathbf{B}}^T\left[\tilde{\mathbf{B}}\dot{\boldsymbol{\lambda}}^g - \mathbf{Y}\frac{d\hat{\boldsymbol{g}}}{ds} - \left(\tilde{\mathbf{B}}\dot{\boldsymbol{\Lambda}}^{\boldsymbol{y}} - \tilde{\mathbf{P}}\right)\frac{d}{ds}(\ln\tilde{\boldsymbol{N}})\right] = \boldsymbol{0}. \tag{40}$$

The usefulness of the decomposition of $d\boldsymbol{\lambda}/ds$ in Eq. (35) is now evident because it ensures that the first term in Eq. (32) is always satisfied, regardless of the value of $d\ln\tilde{\boldsymbol{N}}/ds$.

The phase moles derivatives, $d\ln\tilde{\boldsymbol{N}}/ds$, are determined from the second implicit relation defined in Eq. (32), namely

$$\frac{d}{ds}\left(\tilde{\mathbf{P}}^T\boldsymbol{y}-\tilde{\boldsymbol{N}}\right)=\tilde{\mathbf{P}}^T\left(\tilde{\mathbf{P}}\frac{d}{ds}(\ln\tilde{\boldsymbol{N}})-\mathbf{Y}\frac{d\hat{\boldsymbol{g}}}{ds}+\tilde{\mathbf{B}}\frac{d\boldsymbol{\lambda}}{ds}\right)-\frac{d\tilde{\boldsymbol{N}}}{ds}=0 \tag{41}$$

Making use of the following relationship for $d\ln\tilde{\boldsymbol{N}}/ds$ when $\boldsymbol{R}=\mathbf{0}$,

$$\frac{d}{ds}(\ln\tilde{\boldsymbol{N}})=\operatorname{diag}(\tilde{\boldsymbol{N}})^{-1}\frac{d\tilde{\boldsymbol{N}}}{ds}=(\tilde{\mathbf{P}}^T\tilde{\mathbf{P}})^{-1}\frac{d\tilde{\boldsymbol{N}}}{ds}, \tag{42}$$

and substituting in Eq. (35) for $d\boldsymbol{\lambda}/ds$, Eq. (41) may be written as

$$\tilde{\mathbf{P}}^T\tilde{\mathbf{B}}\dot{\boldsymbol{\Lambda}}^{\boldsymbol{y}}\frac{d}{ds}(\ln\tilde{\boldsymbol{N}})=\tilde{\mathbf{P}}^T\left(\tilde{\mathbf{B}}\dot{\boldsymbol{\lambda}}^{\boldsymbol{g}}-\mathbf{Y}\frac{d\hat{\boldsymbol{g}}}{ds}\right). \tag{43}$$

Eq. (43) represents a linear system of equations for the solution of $d\ln\tilde{\boldsymbol{N}}/ds$. We now introduce the matrix $\mathbf{M}\equiv\tilde{\mathbf{P}}^T\tilde{\mathbf{B}}\dot{\boldsymbol{\Lambda}}^{\boldsymbol{y}}\in\mathbb{R}^{n^{\mathcal{P}}\times n^{\mathcal{P}}}$ for convenience. The structure of this matrix is studied in detail in Appendix A. In particular, $\mathbf{M}$ is symmetric and positive definite when the phase moles are non zero. In fact, the eigenvalues of $\mathbf{M}$, denoted $\beta_1\geq\beta_m\geq\beta_{n^{\mathcal{P}}}$, have the following upper and lower bounds:

$$\tilde{N}_m\geq\beta_m(\mathbf{M})\geq\frac{\beta_m(\mathbf{C}^T\mathbf{C})}{\|\tilde{\mathbf{B}}\|_2^2}\geq 0,\quad\forall\, m\in\mathcal{P}, \tag{44}$$

where $\mathbf{C}\equiv\tilde{\mathbf{B}}^T\tilde{\mathbf{P}}\in\mathbb{R}^{n^{\mathcal{C}}\times n^{\mathcal{P}}}$ has column vectors, $\boldsymbol{c}_m$, which represent the amount of elements or constraint constants which are associated with the phase m. It is trivial to show that $\sum_{m\in\mathcal{P}}\boldsymbol{c}_m=\boldsymbol{c}$. For the single phase case, $\mathbf{M}$ becomes a scalar M and the bounds on the eigenvalues given in Eq. (44) become the bounds on M itself. In this special case, the lower bound on M is readily given as $M\geq\|\boldsymbol{c}\|_2^2/\|\tilde{\mathbf{B}}\|_2^2$, which is strictly positive. In the development of the single phase GFC method, Pope [35] derived a similar equation as Eq. (43) (divided by the total moles of the mixture) and placed an identical lower bound on the scalar quotient (D in Pope's notation) through other means. In Pope's derivation, the physical meaning of the scalar was unknown, and furthermore, the proof of positivity cannot be readily extended to consider multiple phases. However, the eigenvalue analysis given in Appendix A, and whose result is given by the bounds in Eq. (44), directly relates the eigenvalues of $\mathbf{M}$ to the moles in each phase and is applicable to any number of phases (including the single phase case). Furthermore, the upper bound of $\tilde{N}_m$ on the eigenvalues of $\mathbf{M}$ informs a practical method for determining when $\mathbf{M}$ approaches a positive semidefinite matrix.

With a careful treatment of nearly empty phases, Eq. (43) can be solved in a robust and efficient manner using the Cholesky factorization for symmetric positive definite systems, ensuring that the derivatives $d\boldsymbol{\lambda}/ds$ and $d\ln\tilde{\boldsymbol{N}}/ds$ can be determined in a fully robust way.

3.3. Newton's method

As the Euler integration scheme approximates the pseudo-equilibrium path in a linear way, errors may accumulate during the course of the numerical integration. Therefore, after each new solution is obtained in the numerical integration of Eq. (24), Newton's method is used to attempt to reduce the residual below a specified global error tolerance for a fixed value of s (fixed $\hat{\boldsymbol{g}}$). Newton's method corresponds to solving the following linear system for successive updates in the pseudo-equilibrium solution,

$$\mathbf{J}\left(\tilde{\boldsymbol{x}}^{k+1}-\tilde{\boldsymbol{x}}^{k}\right)=-\mathbf{R}(\tilde{\boldsymbol{x}}^{k},\hat{\boldsymbol{g}}), \tag{45}$$

where the superscript k denotes the kth solution iterate and the system Jacobian, $\mathbf{J}$, is determined to be

$$\mathbf{J}\equiv\frac{\partial\mathbf{R}}{\partial\tilde{\boldsymbol{x}}}=\begin{bmatrix}\tilde{\mathbf{B}}^T\tilde{\mathbf{B}} & \tilde{\mathbf{B}}^T\tilde{\mathbf{P}}\\ \tilde{\mathbf{P}}^T\tilde{\mathbf{B}} & \tilde{\mathbf{P}}^T\tilde{\mathbf{P}}\end{bmatrix}-\begin{bmatrix}\mathbf{0} & \mathbf{0}\\ \mathbf{0} & \operatorname{diag}(\tilde{\boldsymbol{N}})\end{bmatrix} \tag{46}$$

Note that the parentheses on the right hand side of Eq. (45) denote that the residual is evaluated at $(\tilde{\boldsymbol{x}}^k,\hat{\boldsymbol{g}})$, while those on the left simply distribute the matrix vector product to both $\tilde{\boldsymbol{x}}^{k+1}$ and $\tilde{\boldsymbol{x}}^k$.

In some situations, the above system may be singular, making it impossible to converge the solution further after taking a continuation step. In such cases, the Newton iterations are abandoned and the residual is reduced by reducing the step-size used for the numerical integration and retaking the step.

3.4. Inclusion of condensed phases

The initialization procedure presented in Section 3.1 typically does a good job of predicting which condensed phases should be present in the equilibrium mixture through the Min-G solution. However, it is possible that the phases present in the initial solution are not the correct ones which minimize the Gibbs free energy. Furthermore, it is also possible that some phases, which are correctly included in the initial solution, are removed during the course of the integration of Eq. (24). Therefore, at the end of the integration of Eq. (24), a check must be performed to determine whether or not a previously neglected phase can in fact minimize the system Gibbs energy further. Since the equilibrium solution represents a stationary point of the Lagrange function ($\partial L=0$), Eq. (12) yields the necessary condition for a new phase to be included. Namely, if

$$\tilde{g}_c-\sum_{i\in\mathcal{C}}\lambda_i^*B_{ci}<0, \tag{47}$$

for any condensed species c, which has not yet been included in the equilibrium solution, then adding the phase to which species c belongs will decrease the overall Gibbs energy at equilibrium. This is sometimes referred to as the vapor pressure test. When multiple phases meet this criteria, the one with the most negative change in the Gibbs energy is added.

When it is determined that a new phase should be included, a phase redistribution procedure is performed which distributes moles of the largest (in terms of quantity) species into the new phase while satisfying the mass balance constraint of Eq. (20). This is done in the following way. First, the current solution of the species moles vector, $\boldsymbol{N}$, is extended by the number of species in the new phase. If the new phase has index m, then the extended species vector, denoted by $\boldsymbol{N}^{\text{ext}}$, is computed as

$$N_j^{\text{ext}}=\begin{cases}N_j, & j\in\mathcal{S}\\ \tilde{N}_m/n_m^{\mathcal{S}}, & j\in\mathcal{S}_m\end{cases}. \tag{48}$$

where $\tilde{N}_m$ is the desired number of initial moles in the phase m, and $n_m^{\mathcal{S}}$ denotes the number of species in that phase. The constraint matrix $\mathbf{B}$, the phase summation matrix $\mathbf{P}$, and the species index set are also extended accordingly.

We then search for an update in the $n^{\mathcal{C}}$ largest species of $\boldsymbol{N}^{\text{ext}}$ which will satisfy the mass balance constraints through the solution of the linear system,

$$\mathbf{B}^T\Delta\boldsymbol{N}^{\max}=\boldsymbol{c}-\mathbf{B}^T\boldsymbol{N}^{\text{ext}}, \tag{49}$$

where the vector $\Delta\boldsymbol{N}^{\max}$ is defined to be a vector of zeros except for the elements representing the $n^{\mathcal{C}}$ largest species. Note that Eq. (49) represents a linear system with $n^{\mathcal{C}}$ equations and $n^{\mathcal{C}}$ unknowns. Furthermore, a suitable update can always be obtained by using the singular value decomposition of the sub matrix of $\mathbf{B}^T$ representing the $n^{\mathcal{C}}$ maximum species, even when that matrix is rank deficient.

Finally, a new initial species moles vector is computed by applying the update to $\boldsymbol{N}^{\text{ext}}$,

$$\boldsymbol{N}(0)=\boldsymbol{N}^{\text{ext}}+\Delta\boldsymbol{N}^{\max}. \tag{50}$$

It is easy to verify that that this new $\boldsymbol{N}(0)$ vector satisfies Eq. (20). With a new $\boldsymbol{N}(0)$, the solution is then reinitialized and the integration procedure is repeated to solve Eq. (24). This whole process must be repeated until all necessary phases are included in the equilibrium mixture according to Eq. (47).

4. Solution algorithm

The previous section detailed the mathematical basis for the MPFGC method. However, in order to create an efficient and robust equilibrium solver, several algorithmic details must be developed. An overview of the full MPFGC algorithm is presented in this section.

For a fixed temperature, pressure, and constraint vector, the initial moles of each species are determined using Eqs. (26)–(28). Following initialization, the proceeding steps are then used to compute the integral in Eq. (24).

1. The initial solution $\hat{\boldsymbol{x}}(0)$ and Gibbs energy vector $\hat{\boldsymbol{g}}(0)$ are computed according to Eqs. (29)–(31). The continuation parameter and step size are also initialized as $s = 0$ and $\Delta s = 1$.
2. Compute the tangent vector of the pseudo-equilibrium path, $d\hat{\boldsymbol{x}}/ds$ at s using Eqs. (35)–(37), and Eq. (43).
3. Next, integrate the solution forward along the pseudo-equilibrium path with an Euler integration over Δs,
$$\tilde{\boldsymbol{x}}^0 = \hat{\boldsymbol{x}}(s) + \frac{d\hat{\boldsymbol{x}}}{ds}\Delta s. \tag{51}$$
The superscript 0 is used to denote the initial iterate for the Newton iteration procedure. The Gibbs energy vector is also updated via Eq. (23) at $s + \Delta s$.
4. Newton's method is then used to reduce the residual vector below a specified tolerance, ϵ_{abs}, using Eq. (45) and (46). The Newton iterations are stopped when either (i) the iterations converge, such that
$$\|\boldsymbol{R}(\tilde{\boldsymbol{x}}^k, \hat{\boldsymbol{g}}(s+\Delta s))\|_2 \leq \epsilon_{\text{abs}}, \tag{52}$$
(ii) a maximum number of iterations is reached, or (iii) the residual norm increases above the norm of the previous iterate.
5. Following the Newton iterations, the new solution vector is tested against the following criteria:
$$\|\boldsymbol{R}(\tilde{\boldsymbol{x}}^k, \hat{\boldsymbol{g}}(s+\Delta s))\|_2 \leq \max\left[(1+\epsilon_{\text{rel}})\left\|\boldsymbol{R}(\hat{\boldsymbol{x}}(s), \hat{\boldsymbol{g}}(s))\right\|_2, \epsilon_{\text{abs}}\right]. \tag{53}$$
If the above inequality holds true, then the iterate k is accepted and the solution is updated as $\hat{\boldsymbol{x}}(s) = \tilde{\boldsymbol{x}}^k$, $s = s + \Delta s$, and the step-size Δs is increased via
$$\Delta s = \min(s - 1,\ 2\Delta s). \tag{54}$$
Otherwise, the solution is not updated and Δs is reduced by a factor of 2 and the algorithm continues at Step 3. Note that the term $(1 + \epsilon_{\text{rel}})$ in Eq. (53) prevents the step-size Δs from decreasing to zero, allowing the solution to progress with a small increase in the residual.
6. If $s = 1$ after the above step, then the solution vector corresponds to the equilibrium solution for the included phases. If not, the solution procedure is continued starting from Step 2.
7. The phase inclusion test is checked to see if any additional phases should be included in the equilibrium mixture, according to Eq. (47). If it is determined that a previously excluded phase can reduce the Gibbs energy of the equilibrium solution, then Eqs. (48)–(50) are used to compute a new initial species moles vector $\boldsymbol{N}(0)$ with the addition of the new phase, and Eq. (24) must be reintegrated starting from Step 1.

Figure 1 provides a graphical overview of the MPGFC method to help clarify the algorithm, of which several aspects are worth elaborating on. To start with, while the Newton iteration procedure attempts to bring the residual below an absolute tolerance, ϵ_{abs}, it is indicated in Step 5 that the solution is accepted as long as Eq. (53) is valid for some small ϵ_{rel}. This is done to allow the integration to proceed for a small enough Δs even when the Newton procedure cannot converge. Typically, if such a situation is encountered, allowing the solution to proceed forward will eventually allow the Newton iterations to converge and maintain an acceptable error tolerance on the solution. In the worst case scenario, the MPGFC method breaks down to a simple Euler integration with small step sizes.

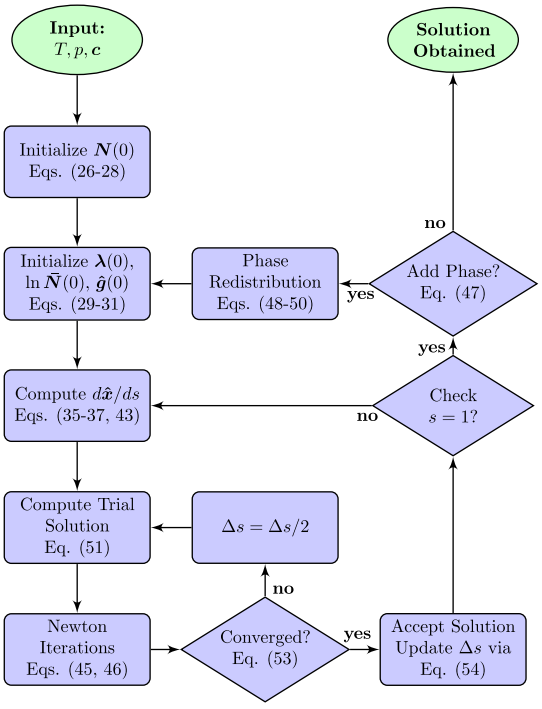

Fig. 1. Flow diagram of the solution procedure for the Multiphase Gibbs Function Continuation method at a given fixed temperature and pressure.

In some cases, a particular phase tends towards zero as the integration in s is computed. Since the robustness of the MPGFC method relies on including only nonempty phases, these phases must be removed when the number of moles fall below some tolerance. Because of this, a small adaptation is included in the Newton procedure which first removes any phases meeting this criteria, before computing the system Jacobian. If the Newton iteration is rejected in Step 5, then the original phase ordering must be remembered. This introduces some extra book keeping in the algorithm, though it does not greatly affect the overall complexity or the necessary coding required to implement it.

Finally, the choice of solution variable $\ln \tilde{\boldsymbol{N}}$ as opposed to $\tilde{\boldsymbol{N}}$ for the phase moles is an important one for two reasons. First, the algebra necessary to develop the method is made more simple. Second, and more importantly, is that this choice automatically guaranties that the phase moles are strictly positive, further guarantying the species moles are strictly positive as well. This makes the necessary coding far easier because negative moles and mole fractions do not have to be dealt with as in other equilibrium solution methods (see for example, CEA [14]).

5. Results and discussion

The MPGFC method has been implemented in the Multicomponent Thermodynamic and Transport Properties for Ionized Gases in C++ (Mutation^{++}) library[2] [43]. Among other things, Mutation^{++} provides thermodynamic properties of individual species and has an option of including the thermodynamic database [16] used in the NASA CEA [14,15] code which will be used for all of the results presented here.

5.1. Constrained single phase mixture

As previously mentioned in the introduction, Bishnu et al. [32] developed a linearly constrained version of the CEA and STANJAN codes and performed several numerical experiments to judge the overall

[2] Available for download at https://www.mutationpp.org .

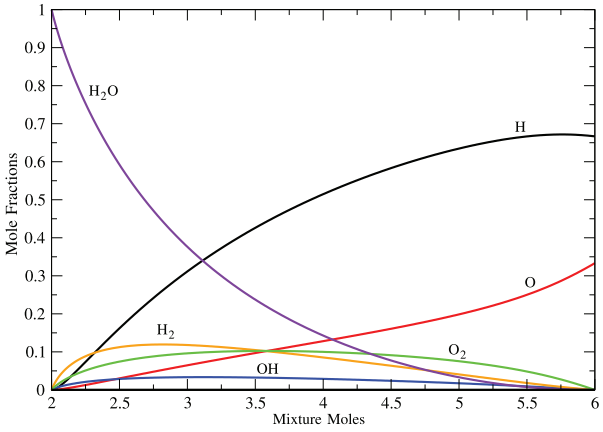

Fig. 2. Water mixture composed of 4 moles of H and 2 moles of O at 1500 K and 1 atm with total number of moles constrained between the limits of 2 and 6 moles.

robustness of the two methods with constraints in addition to the mass balance constraints. One such set of calculations used a simple 8-species H_2O mixture comprised of H, O, OH, H_2, O_2, H_2O, HO_2, and H_2O_2 in which the total moles of the mixture were constrained. This constraint may be written as

$$\sum_{j\in\mathcal{S}} N_j = N_{\text{mix}} \tag{55}$$

Note that this is the same constraint as was used for the example in Table 1.

If the elemental moles of H and O are 4 and 2 mol, respectively, then the above constraint on the total moles of the mixture limits the feasible region of equilibrium solutions to $2 \leq N_{\text{mix}} \leq 6$. On the boundaries of this feasible region, the species moles are determined completely by the constraints themselves: at $N_{\text{mix}} = 2$, $N_{H_2O} = 2$ while all other species are zero, and at $N_{\text{mix}} = 6$, $N_H = 4$ and $N_O = 2$ with the other species zero. Bishnu found that at these boundaries, CEA failed to converge to a solution at 1500 K and 1 atm.

Figure 2 shows the equilibrium mole fractions obtained using the MPGFC method for this H_2O mixture at 1500 K and 1 atm with the mixture moles constrained over the span of the feasible region. It is clear from the figure that the MPGFC method can successfully solve the equilibrium solution even at the boundaries of the feasible region. Perhaps more importantly, the use of the Simplex algorithm when determining the initial conditions (Eqs. (26) and (27)) allows the method to detect when a set of input constraints have no feasible region, and an appropriate error message may be presented to the user.

5.2. A multiphase example

In many fields, multiphase equilibrium solutions are used to make engineering calculations or to understand complex chemical processes. As an example of a multiphase problem, a calculation has been performed with a Silicon–Phenolic mixture which has been used to study complex ablation phenomena occurring at the surface of some ablator materials during atmospheric entry [44]. Figure 3 shows the results of a calculation with the complex Si-C_6H_5OH mixture. Because CEA treats all condensed phases as pure phases, each condensed phase was treated separately in the MPGFC calculation (though the algorithm described here can be used on any general set of ideal phases).

It is clear from Fig. 3 that the results obtained with the MPGFC method compare exactly with those obtained using CEA. It should also be noted that CEA was not able to converge for temperatures below 400 K due to its poor initial estimate of the solution. Therefore, the CEA solution begins at 400 K in Fig. 3.

One interesting feature of the solution is how the solid silicon-oxide transforms between each of its three stable forms. Due to the pure condensed phase assumption, there is a discontinuity in the mole fractions around 1700 K when it becomes more preferential for the Si to combine with C to form solid SiC(β) rather than combining with O to form solid SiO_2 in its β-crystalline state. The carbon needed to form SiC is taken from the graphite when this change occurs, causing a steep drop in the C(gr) mole fraction at 1700 K.

Figure 4 shows the computed eigenvalues of the linear system matrix, $\mathbf{M} \equiv \tilde{\mathbf{P}}^T \tilde{\mathbf{B}} \dot{\mathbf{\Lambda}}^{\boldsymbol{y}}$, from Eq. (43), along with the corresponding eigenvalue bounds given in Eq. (44). It is interesting to note that the eigenvalues tend to stay close to their upper limit, which is equal to the phase moles of the phase corresponding to each eigenvalue. This may be explained by decomposing $\mathbf{M}$ as,

$$\mathbf{M} = \tilde{\mathbf{P}}^T \tilde{\mathbf{P}} + \tilde{\mathbf{P}}^T \boldsymbol{r}^{\boldsymbol{y}}. \tag{56}$$

where $\boldsymbol{r}^{\boldsymbol{y}} = \tilde{\mathbf{B}} \dot{\mathbf{\Lambda}}^{\boldsymbol{y}} - \tilde{\mathbf{P}}$ is the residual of the least squares solution for $\dot{\mathbf{\Lambda}}^{\boldsymbol{y}}$ in Eq. (37). From this, it is easy to see that the mth eigenvalue of $\mathbf{M}$ is exactly

$$\beta_m(\mathbf{M}) = \bar{N}_m + \beta_m(\tilde{\mathbf{P}}^T \boldsymbol{r}^{\boldsymbol{y}}), \tag{57}$$

because $\tilde{\mathbf{P}}^T \tilde{\mathbf{P}}$ is diagonal with diagonal entries equal to the phase moles of each phase. From Eq. (57), it is clear that the eigenvalues of $\mathbf{M}$ tend towards the phase moles as the residual in Eq. (37) decreases. Note also that the mth column of $\boldsymbol{r}^{\boldsymbol{y}}$ is essentially the residual of Eq. (37) corresponding to the phase m. Therefore, when the least squares system can be exactly satisfied for a given phase, the eigenvalue of $\mathbf{M}$ corresponding to that phase is exactly the number of phase moles. In Fig. 4, this is clearly evident for the eigenvalues of the solid phases of SiO_2. Since all of the Si in the equilibrium solution is contained in solid SiO_2 (see Fig. 3), the least squares problem in Eq. (37) corresponding to SiO_2 can be exactly satisfied.

6. Concluding remarks

In this work, the single phase Gibbs function continuation method has been extended to a general multiphase algorithm. To the authors' best knowledge, this represents the first time the Gibbs function continuation method has been extended to a general multiphase system and that the MPGFC method is the first multiphase, constrained equilibrium solution algorithm which is guaranteed to converge for all well posed constraints. The major contributions are listed as follows:

- The phase moles have been added to the solution vector with the necessary mathematical adjustments developed for the GFC methodology.
- A procedure to ensure that the Gibbs phase rule is satisfied has been included in the initialization procedure along with a phase redistribution technique to ensure all phases are correctly included.
- Strictly positive (upper and lower) bounds have been placed on the eigenvalues of the linear system matrix necessary for computing the tangent vector of the pseudo-equilibrium path in a robust manner.
- Furthermore, it was shown that the eigenvalues tend toward the moles of each included phase as the residual of the least squares solution for $\dot{\mathbf{\Lambda}}^{\boldsymbol{y}}$ decreases.
- The eigenvalue analysis has been used to develop a sensible procedure for removing phases from the equilibrium solution, namely when the moles in a phase drop below a specified tolerance.

The MPGFC method has recently been implemented in the MUTATION^{++} library, and the above points have been demonstrated on two numerical test cases which serve to highlight some of the features of the method. A single phase case demonstrated the use of constraints on the equilibrium mixture and the robustness of the method when the solution lies on the edge of the feasible region. A multiphase example was used to show, first and foremost, that the method provides the correct solution when compared to the well established CEA code, and secondly that the underlying eigenvalue analysis is correct.

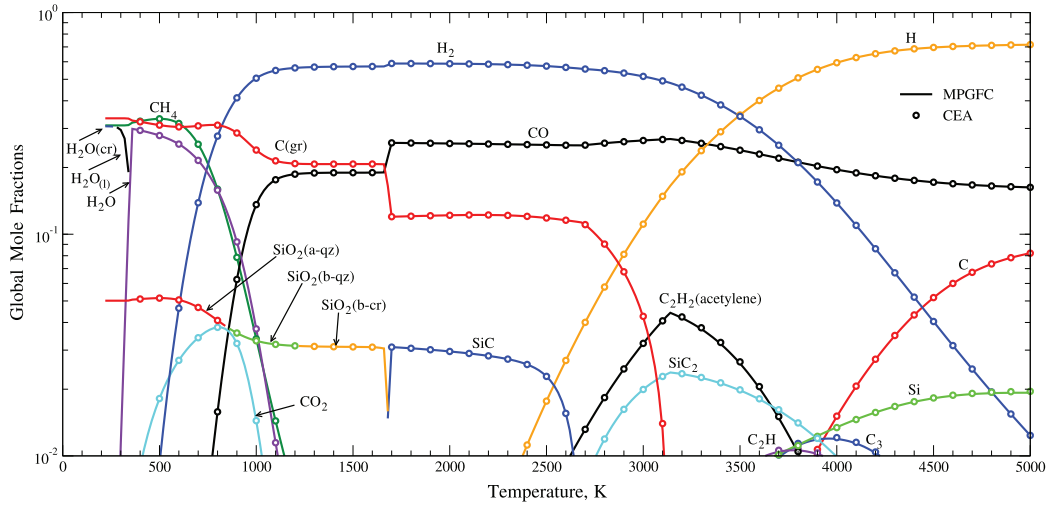

Fig. 3. Global mole fractions of the major equilibrium species for a mixture consisting of 90% Phenol (C_6H_5OH) and 10% Si by moles at 1 atm. Comparison between results obtained with CEA and the MPGFC method. All condensed species are considered as separate, pure phases.

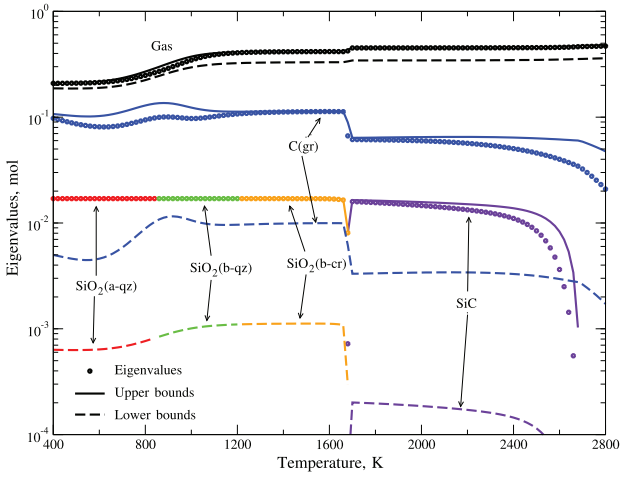

Fig. 4. Eigenvalues of the matrix $\tilde{\mathbf{P}}^T\tilde{\mathbf{B}}\dot{\boldsymbol{\Lambda}}^{\mathbf{y}}$ at $s = 1$ for the equilibrium solution in Fig. (3) with the associated upper and lower bounds from Eq. (44).

Finally, the MPGFC method is shown to be a reliable and robust algorithm for computing linearly constrained, multiphase, chemical equilibrium solutions.

Acknowledgments

This research has been funded through a Fellowship provided by the European Research Council Starting grant #259354: "*Multiphysics models and simulations for reacting and plasma flows applied to the space exploration program.*" The authors would like to thank Benjamin Graille from the Université Paris Sud for many helpful discussions in the early development of the MPGFC method as well as Nagi Mansour from NASA Ames Research Center and Jean Lachaud from the University of California at Santa Cruz for their dedicated testing and encouragement of the development of the equilibrium solver within the MUTATION^{++} library.

Appendix A. Properties of $\tilde{\mathbf{P}}^T\tilde{\mathbf{B}}\dot{\boldsymbol{\Lambda}}^{\mathbf{y}}$

This appendix provides proof of several important properties of the matrix $\tilde{\mathbf{P}}^T\tilde{\mathbf{B}}\dot{\boldsymbol{\Lambda}}^{\mathbf{y}}$ from Eq. (43).

Definition. The so called hat matrix for the least squares problem $\tilde{\mathbf{B}}\dot{\boldsymbol{\Lambda}}^{\mathbf{y}} = \tilde{\mathbf{P}}$ is defined as

$$\mathbf{H} \equiv \tilde{\mathbf{B}}\left(\tilde{\mathbf{B}}^T\tilde{\mathbf{B}}\right)^{-1}\tilde{\mathbf{B}}^T, \tag{A.1}$$

The following results are trivial from the definition of the hat matrix, **H**.

Result 1. **H** is idempotent, meaning $\mathbf{H}^k = \mathbf{H}$ for all powers k and the eigenvalues of **H** are either 0 or 1.

Result 2. **H** is symmetric positive semidefinite, $\mathbf{H} \succeq 0$.

Result 3. The matrix $(\mathbf{I} - \mathbf{H})$ is idempotent and symmetric positive semidefinite, $(\mathbf{I} - \mathbf{H}) \succeq 0$.

Definition. The matrix $\mathbf{M} \in \mathbb{R}^{n^{\mathcal{P}} \times n^{\mathcal{P}}}$ is defined for convenience such that

$$\mathbf{M} \equiv \tilde{\mathbf{P}}^T\tilde{\mathbf{B}}\dot{\boldsymbol{\Lambda}}^{\mathbf{y}}, \tag{A.2}$$

where $\tilde{\mathbf{P}}$ and $\tilde{\mathbf{B}}$ are defined in Eq. (18) and $\dot{\boldsymbol{\Lambda}}^{\mathbf{y}}$ solves the least squares problem, $\tilde{\mathbf{B}}\dot{\boldsymbol{\Lambda}}^{\mathbf{y}} = \tilde{\mathbf{P}}$. We further enforce that $\tilde{\mathbf{B}}$ is full rank, namely $\text{rank}\,(\tilde{\mathbf{B}}) = n^{\mathcal{C}}$.

Result 4. $\mathbf{M} = \tilde{\mathbf{P}}^T\mathbf{H}\tilde{\mathbf{P}}$

Proof. The normal equations solve the least squares problem, $\tilde{\mathbf{B}}\dot{\boldsymbol{\Lambda}}^{\mathbf{y}} = \tilde{\mathbf{P}}$, such that

$$\dot{\boldsymbol{\Lambda}}^{\mathbf{y}} = (\tilde{\mathbf{B}}^T\tilde{\mathbf{B}})^{-1}\tilde{\mathbf{B}}^T\tilde{\mathbf{P}} \tag{A.3}$$

Substituting the above relation into Eq. (A.2) yields the result. □

Result 5. **M** is symmetric positive semidefinite, $\mathbf{M} \succeq 0$.

Proof. This is a trivial result following Results 2 and 4. □

Result 6. When Eq. (19) is satisfied, the kth largest eigenvalue of **M** is upper bounded by the kth largest phase moles, $\beta_k(\mathbf{M}) \leq \bar{N}_k$.

Proof. From Results 3 and 4, we may write

$$\tilde{\mathbf{P}}^T\tilde{\mathbf{P}} - \mathbf{M} = \tilde{\mathbf{P}}^T(\mathbf{I} - \mathbf{H})\tilde{\mathbf{P}} \succeq 0, \tag{A.4}$$

which shows that $\tilde{\mathbf{P}}^T\tilde{\mathbf{P}} \succeq \mathbf{M}$. Therefore, the Courant minimax principle provides that

$$\beta_k(\tilde{\mathbf{P}}^T\tilde{\mathbf{P}}) \geq \beta_k(\mathbf{M}), \tag{A.5}$$

where $\beta_k(\cdot)$ represents the kth largest eigenvalue of the matrix in parentheses. When Eq. (19) is satisfied, $\tilde{\mathbf{P}}^T\tilde{\mathbf{P}} = \text{diag}\,(\bar{\mathbf{N}})$, and $\beta_k(\tilde{\mathbf{P}}^T\tilde{\mathbf{P}}) = \bar{N}_k$ where $\bar{N}_k$ is the phase moles of the kth largest phase. □

Definition. The matrix $\mathbf{C} \in \mathbb{R}^{n^{\mathcal{C}} \times n^{\mathcal{P}}} \equiv \tilde{\mathbf{B}}^T\tilde{\mathbf{P}}$ has column vectors $\mathbf{c}_m = \sum_{k \in \mathcal{S}_m} N_k \tilde{\mathbf{B}}(k, :), \forall\, m \in \mathcal{P}$ which represent the amount of elements (or general constraints) contained in each phase m. Note that $\mathbf{C1} = \sum_{m \in \mathcal{P}} \mathbf{c}_m = \boldsymbol{c}$ where $\boldsymbol{c}$ is the constraint vector from Eq. (9).

Result 7. If $\mathbf{C} \in \mathbb{R}^{n^{\mathcal{C}} \times n^{\mathcal{P}}} \equiv \tilde{\mathbf{B}}^T \tilde{\mathbf{P}}$ has full column rank (meaning $\operatorname{rank} \mathbf{C} = n^{\mathcal{P}}$), then the eigenvalues of $\mathbf{M}$ are lower bounded by the eigenvalues of the matrix $\|\tilde{\mathbf{B}}\|_2^{-2} \mathbf{C}^T \mathbf{C}$ which are strictly positive, $\beta_k(\mathbf{M}) \geq \beta_k(\mathbf{C}^T\mathbf{C})/\|\tilde{\mathbf{B}}\|_2^2 > 0$.

Proof. Letting $\sigma_1 = \|\tilde{\mathbf{B}}\|_2$ denote the largest singular value of $\tilde{\mathbf{B}}$, the difference $\mathbf{M} - \mathbf{C}^T\mathbf{C}/\sigma_1^2$ can be written as

$$\mathbf{M} - \frac{1}{\sigma_1^2}\mathbf{C}^T\mathbf{C} = \mathbf{C}^T\left[(\tilde{\mathbf{B}}^T\tilde{\mathbf{B}})^{-1} - \frac{1}{\sigma_1^2}\mathbf{I}\right]\mathbf{C}. \tag{A.6}$$

The term inside the brackets is symmetric and positive semi-definite because the smallest eigenvalue of $(\tilde{\mathbf{B}}^T\tilde{\mathbf{B}})^{-1}$,

$$\beta_{\min}((\tilde{\mathbf{B}}^T\tilde{\mathbf{B}})^{-1}) = \frac{1}{\beta_{\max}(\tilde{\mathbf{B}}^T\tilde{\mathbf{B}})} = \frac{1}{\sigma_1^2}, \tag{A.7}$$

is equal to the $n^{\mathcal{C}}$ repeated eigenvalue of $\mathbf{I}/\sigma_1^2$. Since $\mathbf{C}$ is full rank, we have

$$\mathbf{M} \succeq \frac{1}{\sigma_1^2}\mathbf{C}^T\mathbf{C}, \tag{A.8}$$

and invoking the Courant minimax principle again yields

$$\beta_k(\mathbf{M}) \geq \frac{1}{\sigma_1^2}\beta_k(\mathbf{C}^T\mathbf{C}). \tag{A.9}$$

Finally, since $\mathbf{C}$ is full rank, the product $\mathbf{C}^T\mathbf{C}$ forms the Gramian of the linearly independent column vectors of $\mathbf{C}$ which is guaranteed to be symmetric positive definite with strictly positive eigenvalues. □

Result 8. When $n^{\mathcal{P}} = 1$, $\mathbf{M} = M$ is a strictly positive scalar with a lower bound, $M \geq \|\boldsymbol{c}\|_2^2/\|\tilde{\mathbf{B}}\|_2^2$.

Proof. From Result 7, with $n^{\mathcal{P}} = 1$, we have easily

$$M = \beta(\mathbf{M}) \geq \frac{1}{\sigma_1^2}\beta(\boldsymbol{c}^T\boldsymbol{c}) = \frac{\|\boldsymbol{c}\|_2^2}{\|\tilde{\mathbf{B}}\|_2^2}. \tag{A.10}$$

□

References

[1] S. Chan, C. Tan, Complex equilibrium calculations by simplex and duality theories with applications to liquid metal fuel propulsion systems, Combust. Flame 88 (2) (1992) 123–136.
[2] R. Pajarre, P. Blomberg, P. Koukkari, Thermochemical multi-phase models applying the constrained Gibbs energy method, Comput.-Aided Chem. Eng. 25 (2008) 883–888.
[3] P. Koukkari, R. Pajarre, A Gibbs energy minimization method for constrained and partial equilibria, Pure Appl. Chem. 83 (6) (2011) 1243–1254.
[4] F.S. Milos, Y.-K. Chen, Comprehensive model for multicomponent ablation thermochemistry, in: AIAA, Aerospace Sciences Meeting and Exhibit (1997).
[5] B.F. Blackwell, M.A. Howard, An element potential based chemical equilibrium solver for gas/surface thermochemistry, in: 50th AIAA Aerospace Sciences Meeting including the New Horizons Forum and Aerospace Exposition, American Institute of Aeronautics and Astronautics, 2012.
[6] J. Rabinovitch, V.M. Marx, G. Blanquart, Pyrolysis gas composition for a phenolic impregnated carbon ablator heatshield, in: 11th AIAA/ASME Joint Thermophysics and Heat Transfer Conference, American Institute of Aeronautics and Astronautics, 2014.
[7] F.V. Zeggeren, S.H. Storey, The computation of chemical equilibria, The Computation of Chemical Equilibria, Cambridge University Press, 1970.
[8] W.R. Smith, R.W. Missen, Chemical reaction equilibrium analysis: theory and algorithms, Chemical Reaction Equilibrium Analysis: Theory and Algorithms, Krieger, Malabar, FL, 1991.
[9] W.B. White, S.M. Johnson, G.B. Dantiz, Chemical equilibrium in complex mixtures, J. Chem. Phys. 28 (5) (1958) 751–755.
[10] K.K. Kuo, Principles of combustion, second edition, John Wiley and Sons, Inc, 2005.
[11] W.B. White, Numerical determination of chemical equilibrium and the partitioning of free energy, J. Chem. Phys. 46 (11) (1967) 4171–4175.
[12] B. Bottin, D.V. Abeele, M. Carbonaro, G. Degrez, G. Sarma, Thermodynamic and transport properties for inductive plasma modeling, J. Thermophys. Heat Transf. 13 (3) (1999) 343–350.
[13] W.C. Reynolds, The Element Potential Method for Chemical Equilibrium Analysis: Implementation in the Interactive Program STANJAN Version 3, Technical Report, Department of Mechanical Engineering, Stanford University, 1986.
[14] S. Gordon, B.J. McBride, Computer Program for Calculations of Complex Chemical Equilibrium Compositions and Aplications: Part 1. Analysis, RP, NASA, 1994.1311
[15] B.J. McBride, S. Gordon, Computer Program for Calculations of Complex Chemical Equilibrium Compositions and Aplications: Part 2. User's Manual and Program Description, RP 1311, NASA, 1996.
[16] B.J. McBride, M.J. Zehe, S. Gordon, NASA Glenn Coefficients for Calculating Thermodynamic Properties of Individual Species, TP 2002-211556, NASA, 2002.
[17] J.C. Keck, D. Gillespie, Rate-controlled partial-equilibrium method for treating reacting gas mixtures, Combust. Flame 17 (2) (1971) 237–241.
[18] A. Morr, J. Heywood, Partial equilibrium model for predicting concentration of CO in combustion, Acta Astronautica 1 (7-8) (1974) 949–966.
[19] M. Delichatsios, J.C. Keck, Rate-controlled constrained-equilibrium calculations of CO and NO freezing in internal combustion engines, in: ACS Division of Petroleum Chemistry Symposium on Chemistry of Combustion in Engines, 20, 1975, pp. 105–113.Philadelphia, PA
[20] R. Law, M. Metghalchi, J.C. Keck, Rate-controlled constrained equilibrium calculation of ignition delay times in hydrogen-oxygen mixtures, Symposium (International) on Combustion 22 (1) (1989) 1705–1713.
[21] J.C. Keck, Rate-controlled constrained-equilibrium theory of chemical reactions in complex systems, Prog. Energy Combust. Sci. 16 (1990) 125–154.
[22] V. Yousefian, A rate-controlled constrained-equilibrium thermochemistry algorithm for complex reacting systems, Combust. Flame 115 (1-2) (1998) 68–80.
[23] D. Hamiroune, P. Bishnu, M. Metghalchi, J.C. Keck, Rate-controlled constrained-equilibrium method using constraint potentials, Combust. Theory Model. 2 (1998) 81–94.
[24] Q. Tang, S.B. Pope, A more accurate projection in the rate-controlled constrained-equilibrium method for dimension reduction of combustion chemistry, Combust. Theory Model. 8 (2004) 255–279.
[25] W. Jones, S. Rigopoulos, Rate-controlled constrained equilibrium: Formulation and application to nonpremixed laminar flames, Combust. Flame 142 (3) (2005) 223–234.
[26] M. Janbozorgi, S. Ugarte, H. Metghalchi, J.C. Keck, Combustion modeling of monocarbon fuels using the rate-controlled constrained-equilibrium method, Combust. Flame 156 (10) (2009) 1871–1885.
[27] M. Janbozorgi, H. Metghalchi, Rate-controlled constrained-equilibrium theory applied to expansion of combustion products in the power stroke of an internal combustion engine, Int. J. Thermodyn 12 (1) (2009) 44–50.
[28] V. Hiremath, Z. Ren, S.B. Pope, A greedy algorithm for species selection in dimension reduction of combustion chemistry, Combust. Theory Model. 14 (5) (2010) 619–652.
[29] V. Hiremath, Z. Ren, S.B. Pope, Combined dimension reduction and tabulation strategy using JSAT–RCCE–GALI for the efficient implementation of combustion chemistry, Combust. Flame 158 (11) (2011) 2113–2127.
[30] G.P. Beretta, J.C. Keck, M. Janbozorgi, H. Metghalchi, The rate-controlled constrained-equilibrium approach to far-from-local-equilibrium thermodynamics, Entropy 14 (12) (2012) 92–130.
[31] S. Elbahloul, S. Rigopoulos, Rate-controlled constrained-equilibrium (RCCE) simulations of turbulent partially premixed flames (Sandia D/E/F) and comparison with detailed chemistry, Combust. Flame 162 (5) (2015) 2256–2271.
[32] P.S. Bishnu, D. Hamiroune, M. Metghalchi, J.C. Keck, Contrained-equilibrium calculations for chemical systems subject to generalized linear constraints using the NASA and STANJAN equilibrium programs, Combust. Theory Model. 1 (1997) 295–312.
[33] P. Bishnu, D. Hamiroune, M. Metghalchi, Development of constrained equilibrium codes and their applications in nonequilibrium thermodynamics, J. Energy Resour. Technol. 123 (3) (2001) 214–220.
[34] S.B. Pope, The Computation of Constrained and Unconstrained Equilibrium Compositions of Ideal Gas Mixtures using Gibbs Function Continuation, 2003, (FDA 03–02).
[35] S.B. Pope, Gibbs function continuation for the stable computation of chemical equilibrium, Combust. Flame 139 (2004) 222–226.
[36] Z. Ren, G.M. Goldin, V. Hiremath, S.B. Pope, Simulations of a turbulent nonpremixed flame using combined dimension reduction and tabulation for combustion chemistry, Fuel 105 (2013) 636–644.
[37] J. Cai, M. Handa, M.F. Modest, Eulerian-eulerian multi-fluid methods for pulverized coal flames with nongray radiation, Combust. Flame 162 (4) (2015) 1550–1565.
[38] M. Kooshkbaghi, C.E. Frouzakis, E. Chiavazzo, K. Boulouchos, I.V. Karlin, The global relaxation redistribution method for reduction of combustion kinetics, J. Chem. Phys. 141 (4) (2014) 044102.
[39] T.C. Kelley, Iterative methods for linear and nonlinear equations, Society for Industrial and Applied Mathematics, 1995.
[40] D.B. Shear, Stability and uniqueness of the equilibrium point in chemical reaction systems, J. Chem. Phys. 48 (9) (1968) 4144.
[41] W.H. Press, S.A. Teukolsky, W.T. Vetterling, B.P. Flannery, Numerical Recipes in C: The Art of Scientific Computing, 2nd, Cambridge University Press, 1992.
[42] J.W. Gibbs, The equilibrium of heterogeneous substances, Trans. Conn. Acad. Arts Sci. 111 (1874) 198–248.
[43] J.B. Scoggins, T.E. Magin, Development of mutation++, multicomponent thermodynamic and transport properties for ionized gases library in C++, in: 11th AIAA/ASME Joint Thermophysics and Heat Transfer Conference, American Institute of Aeronautics and Astronautics, 2014, doi:10.2514/6.2014-2966.
[44] B. Helber, C.O. Asma, Y. Babou, A. Hubin, O. Chazot, T.E. Magin, Material response characterization of a low-density carbon composite ablator in high-enthalpy plasma flows, J. Mater. Sci. 49 (13) (2014) 4530–4543, doi:10.1007/s10853-014-8153-z.